Analyst

PAPER

Cite this: *Analyst*, 2023, **148**, 4064

Microfluidic encapsulation of DNAs in liquid beads for digital PCR application

Fariba Malekpour Galogahi, Melody Christie, Ajeet Singh Yadav, Hongjie An, Helen Stratton and Nam-Trung Nguyen *

Droplet-based microfluidics and digital polymerase chain reaction (PCR) hold significant promise for accurately detecting and quantifying pathogens. However, existing droplet-based digital PCR (ddPCR) applications have been relying exclusively on single emulsion droplets. Single emulsion droplets may not be suitable for applications such as identifying the source and pathways of water contamination where the templates must be protected against harsh environmental conditions. In this study, we developed a core–shell particle to serve as a protective framework for DNAs, with potential applications in digital PCR. We employed a high-throughput and facile flow-focusing microfluidic device to generate liquid beads, core–shell particles with liquid cores, which provided precise control over process parameters and consequently particle characteristics. Notably, the interfacial interaction between the core and shell liquids could be adjusted without adding surfactants to either phase. As maintaining stability is essential for ensuring the accuracy of digital PCR (dPCR), we investigated parameters that affect the stability of core–shell droplets, including surfactants in the continuous phase and core density. As a proof of concept, we encapsulated a series of human faecal DNA samples in the core–shell droplets and the subsequent liquid beads. The core–shell particles ensure contamination-free encapsulation of DNA in the core. The volume of the core droplets containing the PCR mixture is only 0.12 nL. Our experimental results indicate that the liquid beads formulated using our technique can amplify the encapsulated DNA and be used for digital PCR without interfering with the fluorescence signal. We successfully demonstrated the ability to detect and quantify DNA under varying concentrations. These findings provide new insights and a step change in digital PCR that could benefit various applications, including the detection and tracking of environmental pollution.

Received 30th May 2023,
Accepted 6th July 2023

DOI: 10.1039/d3an00868a

rsc.li/analyst

Introduction

Human and animal faecal pollution remarkably impacts environmental water quality and represents a direct threat to the health of humans and livestock. Faecal pollution can significantly affect marine harvesting or recreational activities such as swimming.[1] Human and warm-blooded animal faeces contain pathogens that are the main sources of waterborne diseases. Most waterborne pathogens can reside in both human and animal feces.[2] Identifying the source of contamination is crucial for efficient resource management, remediation, and potential environmental risk assessment. Conventional culturing methods for the detection of pathogens are costly, time-consuming, laborious, and inappropriate for prompt prevention of major epidemic outbreaks due to the requirement of long hours of culture.[3] Recently, culture-independent approaches such as surface plasmonic resonance (SPR), DNA microarray, enzyme-linked immunosorbent assay (ELISA), real-time quantitative polymerase chain reaction (qPCR) and digital (dPCR) polymerase chain reaction have been developed to assess waterborne pathogens.[3] Among these techniques, polymerase chain reaction (PCR) is most promising due to its speed, particular sensitivity, and ability to quantify pathogen-specific genes. This technique is based on the enumeration of faecal indicator pathogens such as *Escherichia coli* (*E. coli*) and bacteroidales.[4,5]

Most recently, digital PCR has attracted increasing attention because of its ability of sensitive detection[6] and absolute quantification of pathogens with high selectivity.[7] Digital PCR is based on the division of dilute target template samples into separate low-volume PCR partitions, in which the average template concentration is either at least one or no target molecule.[8] The template quantities are estimated from the number of partitions, indicating a positive signal on the basis of Poisson statistics. Unlike qPCR, digital PCR enables the absol-

Queensland Micro- and Nanotechnology Centre, Griffith University, 170 Kessels Road, Nathan, Queensland 4111, Australia.
E-mail: nam-trung.nguyen@griffith.edu.au

ute quantification of the target template without the need for standard quantification curves. Imperfect amplification efficiencies can impact the cycle threshold (CT) values of the standard curve and consequently reduces the quantification accuracy.[3,9] Compared to qPCR, digital PCR is also more sensitive and precise, when only a limited number of target templates exist in a sample.[3] Droplet digital PCR (ddPCR) is a new generation of digital PCR, where droplets generated using a microfluidic device are used as a reaction chamber for the PCR. Microfluidic technology can address the problem of serial dilution by automatically partitioning genetic targets into a large number of picolitre reaction volumes. Digital PCR platforms based on microfluidics can overcome the drawbacks of sample reagent waste and human errors.[10] A microfluidic device can generate thousands to millions of droplets of picolitre volumes with a formation rate up to several kilohertz. ddPCR demonstrates notable advantages in terms of time saving, cost effectiveness,[11] and high throughput, while maintaining exceptional sensitivity[12] and mitigating the risk of cross-contamination.[13]

ddPCR has been widely utilized in diverse fields such as medical diagnosis,[14] molecular diagnosis,[15] gene sequencing,[16] environmental engineering,[3] and food and feed analysis.[17] However, all these applications have been relying on water-in-oil single-emulsion droplets. For example, Malic *et al.*[18] and Zhao *et al.*[19] employed single droplet digital PCR to quantify epigenetic-based white blood cell differentials and the gene fragment of the epidermal growth factor receptor, respectively. Single emulsion droplets are not suitable for applications where the target DNA needs to be protected from harsh external conditions. For instance, when tracing the source or studying migration patterns of pollutants in water, soil, and atmosphere,[20,21] DNA tracers must be shielded from physical, mechanical and chemical degradation due to high temperature,[22] radicals and UV irradiation,[23,24] high shear forces,[25] oxidative stress,[26] enzymatic degradation,[21] ionizing radiation, extreme pH,[27,28] and strong microorganism activity.[20] The best approach to tackle this issue is the encapsulation and condensation of DNA tracers within a protective shell framework.[29] The shell can enhance DNA tracer stability in interactions with external factors, leading to high recovery rates and stronger detection signals. Pang *et al.* encapsulated synthetic DNA tracers in particles to monitor polluted surface water, groundwater, and soils. The encapsulation process offered protection against various potential risks, including environmental stressors and negative charges. This protective measure significantly enhanced the stability and effectiveness of the DNA tracers, enabling accurate and reliable monitoring under diverse environmental conditions.[30] DNA tags have gained significant attention in recent years for ensuring food safety and product authenticity. Among various methods, encapsulating DNA tags in particles is considered the most effective approach for tracing food products like milk, yogurt, and cheese. The encapsulation approach provides essential protection for the DNA tags. Moreover, the encapsulated DNA tags can be directly identified using digital PCR, eliminating the requirement of extraction from particles, and offering a rapid and precise method of verification.[31]

On the other hand, droplet microfluidics enables the generation of multilayer particles, in which molecules can be selectively and separately encapsulated. Droplet microfluidics demonstrates considerable advantages over conventional techniques for encapsulating DNA. This technology can overcome the bottlenecks of conventional DNA encapsulation approaches such as photopolymerization,[32] interfacial reaction,[33] and layer-by-layer (LBL) assembly.[23] All conventional bulk approaches are commonly associated with reproducibility limitations, limited control of quality and characteristics such as particle size,[34] dispersity, and structures, and high materials consumption.[35] The LBL technique is the most widely used technique and usually results in the incorporation of DNA into multiple layers of matrices during their deposition.[36,37] Liquid beads form when the shell of core–shell droplets is hardened through polymerisation and serve as robust microscale capsules. Liquid beads generated using microfluidics have the potential to be used for digital PCR. DNA encapsulated into liquid beads could be identified effectively by dPCR analysis, without being released from the shell. dPCR can allow for the identification of DNA tracers at a minimum concentration.

Nevertheless, there are some drawbacks associated with the microfluidics technique. The main challenge encountered is developing a stable microfluidic device with reliable hydrophobic and hydrophilic sections.[38] Another barrier to implementing droplet microfluidics is the instability and tendency of the droplets to coalesce during their generation.[39] Consequently, the usage of surfactants for stabilizing the droplets is inevitable. However, most surfactants are environmentally unfriendly, carcinogenic,[40] and highly toxic to humans.[41] Furthermore, droplet microfluidics requires a high level of microfluidic hardware and skill, because of its multidisciplinary nature and complexity. These problems further hinder the rapid commercialization of droplet-based microfluidics.[42,43]

Our present study aims to develop a microfluidic liquid bead platform as a DNA compartmentalisation framework for digital PCR toward applications in water pollution monitoring. We used a PDMS flow-focusing microfluidic system to generate stable core–shell microparticles. We demonstrated that the interaction between phases can be adjusted without adding any surfactants to the core and the shell phases. We further demonstrated that stabilizing droplets can easily be modulated by varying the surfactant concentration in the continuous phase. We also investigated the effect of the density of the core phase on the stability of the core–shell droplets. Finally, we validated the application of the digital PCR based on liquid beads formed from the core–shell droplets for assessing pathogen contamination of water by encapsulating faecal DNA and performing a PCR assay. The developed assay was examined against different concentrations of standard DNA extracted from bacteria, using an AllBac general faecal DNA marker.

Materials and methods

Fabrication of the microfluidic device

A silicon wafer mould was fabricated by photolithography and hard baking of the thick photoresists SU8. The polydimethylsiloxane (PDMS) microfluidic device was fabricated using the soft lithography technique.[44] The PDMS base and curing agent were mixed in a ratio of 10 : 1. After degassing in a desiccator, the mixture was poured into the master mould and cured at 75 °C in an oven for 2 h. The PDMS slab was then peeled off from the master mould. The inlets and outlet were subsequently created using a biopsy punch. Finally, the cleaned PDMS slab was bonded to a glass slide following an oxygen plasma treatment step (PDC-32G-2, Harrick Plasma) for 120 s at 1.2 mbar.

A partial hydrophilic surface modification of the microchannels was accomplished by manually introducing a polyvinyl acetate (PVA) solution of 1 wt% immediately after the device assembly. For partial hydrophilic surface treatment, the PVA coating of hydrophobic channels was prevented by simultaneous injection of air into the hydrophobic channels using a syringe pump at a flow rate of 400 μL min^{-1}. After blowing out the PVA solution with a strong airflow for 15 minutes, the device was annealed at approximately 100 °C for 15 minutes. The process was repeated three times to achieve adequate hydrophilicity. Subsequently, the water repellent agent Aquapel was manually introduced through the hydrophobic channels for 5 min. The channels that should remain hydrophilic were blocked by injecting air using a syringe pump at a flow rate of 800 μL min^{-1}. Finally, Aquapel was entirely removed by blowing air.

Preparation of core–shell particles

Fig. 1 illustrates the flow-focusing geometries used for the generation of core–shell droplets.[45] The device consists of three flow-focusing junctions, a dispersed phase inlet (inlet 1), a shell phase inlet (inlet 2), two continuous phase inlets (inlet 3 and 4), a spacer phase inlet (inlet 5), and an outlet. The widths of the first channel constriction, spiral channel, and all other channels are 30 μm, 400 μm, and 100 μm, respectively. All channels have a uniform depth of 120 μm. The first inlet introduced the core phase that intersected the shell phase flowing through the second inlet at the first junction. The generated core droplets then encountered the second junction to be encapsulated by the shell phase. At the second junction, the shell phase was dispersed using the continuous phase entering from the third and fourth inlets. The generated core–shell droplets then moved to the third junction. At this junction, the droplets were dispersed further by the spacer phase to prevent accidental coalescence. Downstream of the third junction is followed by a spiral channel and the outlet. The core–shell particles were collected in a Petri dish. The collected core–shell particles were subsequently exposed to blue light (450–490 nm, 110–240 V, 24 W) for 20 minutes for complete polymerisation. The choice of blue light for curing specifically aimed at minimizing potential DNA damage that may be caused by UV radiation. Polymerization and subsequent solidification of the shell prevented the coalescence of sample droplets during the subsequent PCR process and ensured their long-term stability.[46,47]

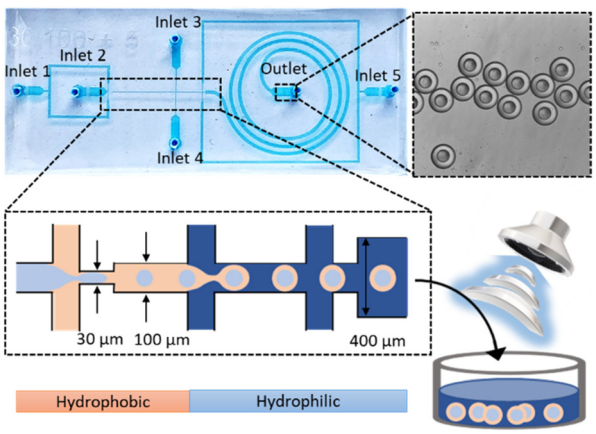

Fig. 1 Five-inlet microfluidic device for the generation of core–shell droplets and liquid beads. Inlet 1: aqueous core fluid; inlet 2: TMPTMA; inlets 3, 4, and 5: aqueous solution containing 50% v/v glycerol and Tween 20.

In the present study, we utilised several liquid systems to study the impact of material properties on the position of the core in the shell droplet. We first studied the surfactant concentration in the continuous phases introduced from inlets 3 and 4 as the spacer fluid, while deionized water was used as the core phase. The continuous phase solutions were prepared by dissolving 50% v/v glycerol and Tween 20 at concentrations of 10^{-3} mol l^{-1} and 10^{-4} mol l^{-1} in deionised water. Adding glycerol (dynamic viscosity of glycerol is $\eta_{glycerol}$ = 6 cP) to water increases the viscosity of the fluid and consequently the shear stress at the second junction, and enhances the detachment of the shell. Tween 20 was chosen as a surfactant because of its non-ionic properties and biocompatibility. This surfactant decreases the shell/continuous phase interfacial tension and stabilises the core–shell droplets. Tween 20 also has a high Hydrophilic Lipophilic Balance (HLB) value of 16.7, promoting shell formation in aqueous emulsion. In the next experiment, 50% v/v glycerol with 10^{-3} mol l^{-1} Tween 20 was used as the continuous phase, and a number of aqueous solutions, including deionised water and glycerol/water mixtures (25% v/v and 50% v/v), were chosen as the core phase, respectively. We utilised TMPTMA as the shell phase in all experiments. TMPTMA is slightly transparent, thermally stable,[48] non-toxic, and biocompatible[49] and has a high-crosslinking capacity.[50] The surface tensions of all phases were measured using a tensiometer through the pendent drop technique (Theta Flex from Biolin Scientific, Gothenburg, Sweden).

All fluids were separately injected using a syringe pump (NEM-B101-03 A, CETONI GmbH, Germany) at a controlled flow rate. For each set of experiments, the flow rates of the core, shell, continuous, and spacer phases were 30 μL h^{-1}, 120 μL h^{-1}, 400 μL h^{-1}, and 400 μL h^{-1}, respectively. An

inverted microscope (Nikon, Eclipse Ti) equipped with a high-speed camera (Phantom Miro3, Vision Research) was used to monitor the generation of droplets in the device. We then investigated video frames captured from the droplet generations using ImageJ. A fluorescence microscope (Eclipse Ti2, Nikon) was used to visualise the overall morphology of the core–shell particles after collection. The 3D morphology of core–shell particles was characterised using scanning electron microscopy (SEM) (JSM-6510LV, JEOL) at an accelerating voltage of 10 kV and a filament current of 65 μA.

Preparation of a mixture for dPCR

Detection of *Bacteroidales* 16S rRNA genes from DNA extracts was performed using AllBac primers. DNA was extracted from a faecal sample of a healthy individual using a QIAamp DNA stool mini kit (Qiagen). Three independent serial dilutions of DNA were tested to determine the sensitivities of the analyses. A 20 μl PCR mixture contained 15 pmol of the primers AllBac296F and AllBac467R, 10 μl of SYBR Green Supermix mix, and 2 μl of DNA at concentrations of 37.88 ng μL^{-1}, 18.94 ng μL^{-1}, 9.47 ng μl^{-1}, and 0.947 ng μl^{-1} as well as 4 μl of DNase-free water to bring to the required volume. All components were mixed exactly before encapsulation.

RT-qPCR

A total mixture volume of 20 μL consisted of 10 μL of Supermix, 2 μL of forward and reverse primers, 2 μL of template DNA (9.47 ng μL^{-1}), and 4 μL of nuclease-free water. RT-qPCR analysis was performed using SYBR Green Supermix PCR under thermal cycle conditions: a PCR initial activation step for 10 min at 95 °C and 3 step-cycling: denaturation for 30 s at 95 °C, annealing for 60 s at 53 °C, and extension for 60 s at 60 °C, for 40 cycles. We used a standard curve consisting of eight serial dilutions of DNA from 13 980 000 copies per reaction to 1.398 copies per reaction. The negative control included the reaction mixture in the absence of DNA. All reactions were performed in triplicate.

dPCR

To encapsulate the PCR mixture, we introduced the mixture as a core phase from the first inlet using a syringe pump. We used TMPTMA and the mixture of 50% v/v glycerol and 10^{-3} mol l^{-1} Tween 20 as the shell phase and the continuous and spacer phases, respectively. The flow rates of the core, shell, continuous, and spacer phases were 10 μL h^{-1}, 100 μL h^{-1}, 200 μL h^{-1}, and 200 μL h^{-1}, respectively. The outlet liquid beads were collected in PCR tubes. The collected samples were subsequently moved to a thermocycler for thermal cycling. PCR cycling conditions were 95 °C for 10 min, followed by 40 cycles at 95 °C for 30 s, 53 °C for 60 s, and 60 °C for 60 s performed in a conventional thermocycler (Bio-Rad CFX Connect, NSW, Australia). After the completion of thermal cycling, the liquid beads were transferred to a Petri dish which was pre-filled with water. The Petri dish was gently held in an angle to allow a uniform monolayer of beads to form for imaging. Bright field and fluorescence microscopy images of particles were then taken with an ECLIPSE Ti2 inverted microscope. The images were analysed using the ImageJ software and Python (v3.9.5) was used to count the number of positive and negative beads. Subsequently, the concentration of the target DNA was calculated according to the Poisson distribution principle:

$$C = -\ln(1 - (P/G))/V, \quad (1)$$

where P is the number of positive particles, G is the number of total particles, and V is the volume of the core droplets.

Results and discussion

Stability of core–shell droplets

Surfactant-free water/oil/water double-emulsions are intrinsically thermodynamically unstable against phase inversion or coalescence. Thus, the use of surfactants in the generation of water/oil/water double-emulsions is inevitable to prolong the lifetime of droplets.[51] In a previous study, we utilised cetyltrimethylammonium bromide (CTAB) as a surfactant in the continuous phase to generate liquid beads. However, we observed that some of these liquid beads suffered from a lack of concentricity inside the shell and partial stability. In addition, some droplets lost their core while passing through the outlet tubing. Furthermore, we found that the eccentric liquid beads released the core contents under heating and the load from the thinner part of the shell earlier than expected. As a result, we need to overcome the destabilization of droplets to produce robust liquid beads suitable for digital PCR. This is critical because the loss of the core and rupturing of the shell during amplification under thermocycling have an adverse effect on the accuracy and sensitivity of dPCR. In the current study, we investigated the effect of Tween 20 as a surfactant in the continuous phase on the concentricity and stability of core–shell droplets. Before adding Tween 20 to the aqueous glycerol solution (surface tension γ = 66.6 mN m^{-1}), all core–shell droplets lost their core to the continuous phase immediately after the formation. At a low Tween 20 concentration (10^{-4} mol l^{-1}) (γ = 52.73 mN m^{-1}), rapid coalescence of the core–shell droplets occurred, and most core droplets were released while passing through the microchannels or in the outlet. By increasing the concentration of Tween 20 to 10^{-3} mol l^{-1} (γ = 40.013 mN m^{-1}), coalescence between droplets occurred less frequently, and the core–shell droplets remained entirely stable, Fig. 2. This phenomenon was attributed to the decrease in the interfacial tension between the shell and continuous phase $\gamma_{\text{shell-Con.}}$ by aligning at the interface of the continuous shell phase.

Absorption of surfactants can also develop a physical barrier against merging of the core droplet to the continuous phase. Double-emulsion droplets are thermodynamically stable if the spreading parameter of the shell phase $S_{\text{shell}} = \gamma_{\text{core-Con.}} - (\gamma_{\text{shell–core}} + \gamma_{\text{shell-Con.}}) > 0$. However, the S_{shell} of the water/oil/water droplets is inherently negative because the tension of the core and continuous phase interface $\gamma_{\text{core-Con.}}$ is

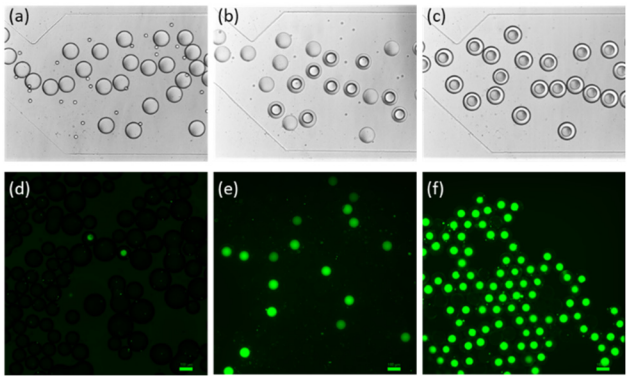

Fig. 2 Bright-field and fluorescence images of the outlet and collected core–shell droplets (a and d) before adding Tween 20; (b and e) at a low Tween 20 concentration (10^{-4} mol l^{-1}); and (c and f) a high Tween 20 concentration (10^{-3} mol l^{-1}), respectively. Scale bar represents 100 μm.

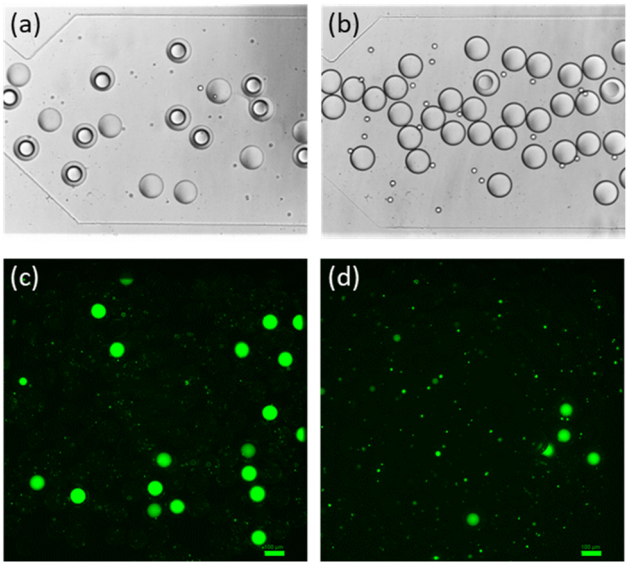

Fig. 3 Bright-field and fluorescence images of outlet and collected core–shell droplets at the concentrations of 25% v/v (a and c) and 50% v/v (b and d), respectively. Scale bar represents 100 μm.

less than either the tension of the shell and core phase interface $\gamma_{\text{shell–core}}$ or the tension of the shell and continuous phase interface $\gamma_{\text{shell-Con.}}$. If the core–shell droplets are formed, the shell dewets the core and the droplets eventually transform into oil/water droplets to minimise the interfacial energy.[52] Adding Tween 20 to the continuous phase reduced $\gamma_{\text{shell-Con.}}$, increasing S_{shell}. Therefore, the shell phase engulfs more adequately the core phase and prevents the core droplet and continuous phases from meeting each other. In addition, the results indicate that Tween 20 leads to better droplet stability than CTAB. This can be justified based on the surfactants' hydrophilic–lipophilic balance (HLB). Tween 20 with more hydrophilicity (HLB = 16.7) contributes more efficiently to stabilising the external interface than CTAB with less hydrophobicity (HLB = 1).

We also investigated the impact of core phase density on the stabilisation of core–shell droplets. As the PCR mixture has a different density from water, it may affect the stability of the droplets, causing shell droplets to lose the core while passing through the microchannels or at the outlet (Fig. 3(a, b, c and d)). The instability of the droplets may be caused by the increasing density through glycerol. It is clear from the results that increasing the core density results in faster destabilisation and coalescence of the core droplet to the continuous phase. This phenomenon can be described with the Archimedes number:

$$\text{Ar} = g{d_{\text{core}}}^3 \rho_{\text{core}} (\rho_{\text{core}} - \rho_{\text{shell}}) / {\mu_{\text{shell}}}^2,$$

where g, d_{core}, μ_{shell}, ρ_{core}, and ρ_{shell} are the acceleration of gravity, core diameter, viscosity of the shell, and core and shell densities, respectively. The Ar number represents the relative effect of gravitational force on viscous force.[53,54] A greater Ar value indicates the more dominant impact of core density and density difference on expediting core droplet movement. Adding glycerol increases Ar by increasing the difference between the core and shell densities. As a result, gravitational forces driven by the density difference accelerate the motion of the core droplet towards the shell interface.

PCR

Initially, we performed RT-qPCR with a dilution of 9.47 ng μL^{-1} to assess the PCR mixture and compare the results to dPCR results. The RT-qPCR predicted a number of 1677.1 copies per microlitre (μL) reaction. In the next step, we utilised an optimised formulation to generate core–shell particles loaded with DNA for dPCR application. Microfluidics technology enabled the encapsulation of DNA into thousands of monodisperse core–shell particles, effectively shielding the DNA from the external environment. These particles acted as reaction chambers for PCR, allowing precise and controlled amplification of DNA samples. During the post-PCR analysis, particles containing DNA emitted fluorescence, while those without DNA remained faint, facilitating the absolute detection and quantification of DNA copies. Due to the high concentration of extracted DNA of 94.7 ng μL^{-1}, there was a possibility of all beads emitting fluorescence, which could lead to an unreliable analysis. Thus, we initiated the process with a 2.5-fold dilution of DNA in the reaction mixture. To demonstrate the sensitive and accurate quantitative measurement of digital PCR using our core–shell particles, we tested several dilutions of DNA solutions ranging from 37.88 ngμL^{-1} to 0.947 ng μL^{-1}. We verified the specificity of the dPCR by utilising liquid beads without a DNA template as a negative control. For each experimental run, we randomly selected hundreds of core–shell particles and captured their fluorescence images for enumeration analysis. As there might be more than one DNA molecule encapsulated in each particle, we calculated the number of DNA copies using mathematical correction of Poisson statistics. We then estimated the concentration of DNA based on the core droplet volume, which is approximately 0.12 nL. Fig. 4(a) illustrates a set of fluorescence images of

thermocycled microfluidic particles containing DNA with varying concentrations.

The negative control particles remained dim during amplification, while increasing the DNA template concentrations in the PCR mixture proportionally enhanced the fraction of positive particles. The images indicated that the microfluidic digital PCR based on liquid beads succeeded without interference in the fluorescence signal by the shell layer. The non-uniformity of the fluorescence signal in the images can likely be attributed to two factors: the non-uniform shape of the core within the shell and the varying positions of the core droplets within the shell. Firstly, the irregular shape of the core can introduce variations in the signal intensity across the shell. Additionally, the lack of centricity of the core within the shell may further impact the fluorescence signals. We employed a customised image processing algorithm to take all these factors into consideration and to achieve robust evaluation.[46,47] The results also demonstrated that all DNA molecules were encapsulated into the core without contaminating the shell. Fig. 4(b) illustrates the comparison between the measured concentrations of DNAs and the expected concentrations. The measured concentrations for each DNA exhibited a high degree of correlation with the expected concentrations. More importantly, the concentration measured

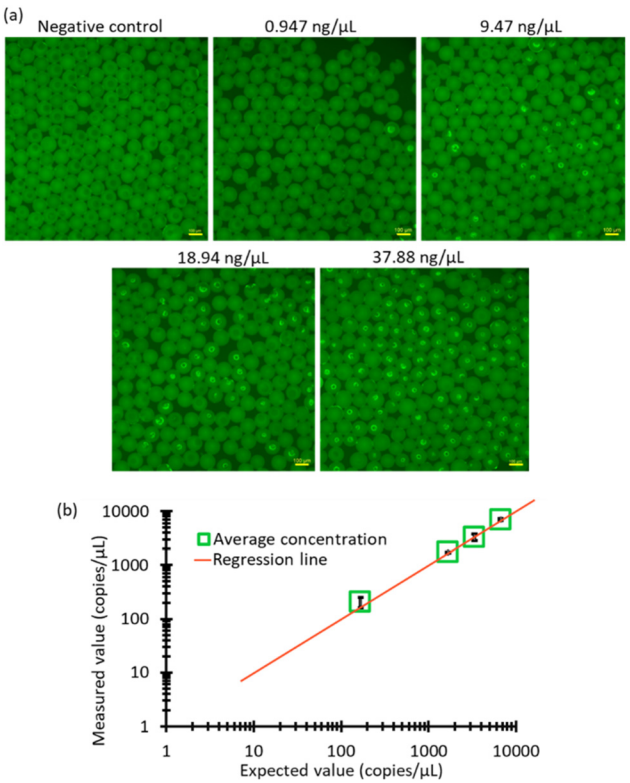

Fig. 4 PCR results of liquid beads: (a) fluorescence microscopy images of core–shell particles without DNA and containing serial dilutions of the DNA template at 0.947, 9.47, 18.94, and 37.88 ng μL^{-1}. Scale bars are 100 μm. (b) Relationship between the measured and expected DNA concentration values in logarithmic scale.

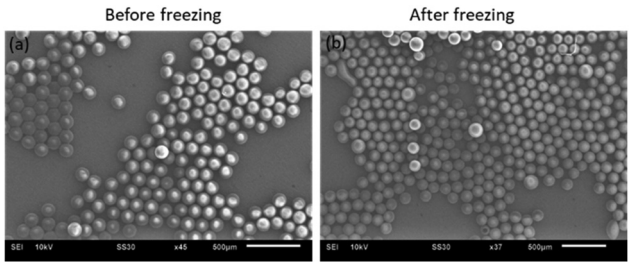

Fig. 5 Scanning electron microscopy images of particles before and after freezing. Scale bars are 500 μm.

with digital PCR (dPCR) at 9.47 ng μL^{-1} was found to be in close agreement with the concentration obtained by RT-qPCR. These findings underscore the potential of the digital PCR system based on liquid beads for detecting pathogenic bacteria and accurately quantifying gene targets. Our observations indicated that the particles remained stable and retained their morphology and structure during the entire process, including generation, thermal cycling, and analysis. Notably, the particles maintained their stability even after prolonged storage in a freezer (Fig. 5), suggesting their potential suitability for applications that require long-term preservation of genetic materials or further analysis.

Conclusion

We demonstrated the generation of stable liquid beads, core–shell particles having a liquid core, without adding any surfactants to the core and shell phases using a microfluidic flow-focusing configuration. We demonstrated that the stabilization of core–shell droplets significantly depends on the hydrophilic–lipophilic balance and concentration of the surfactant in the continuous phase. A surfactant with a greater HLB resulted in better core–shell droplets with aqueous core stability. We further demonstrated that the denser core phase led to faster destabilizing and merging of the core droplet to the continuous phase. Subsequently, we applied the optimised core–shell particles for digital PCR for the purpose of monitoring faecal contamination in environmental water. We efficiently encapsulated a series of DNA dilutions into the core of the liquid beads. DNA molecules were efficiently amplified in the beads, enabling the accurate detection and quantification of DNA molecules. We observed no interference in the fluorescence signal by the shell layer during post-PCR analysis. The usage of the liquid bead to encapsulate DNA overcomes the problem of droplet evaporation during thermal cycling. Based on our previous studies, the shell layer has the potential to protect DNA against physical and mechanical degradation. Comparison of the results obtained from dPCR and RT-qPCR indicated agreement for liquid bead assay efficiency and quantification. The results of this study offer a foundation for expanding the application of dPCR beyond its traditional function of detecting and quantifying genetic targets. Our techno-

logy can now be applied to situations where genetic cargoes need protection, such as tracing of the environmental pollution and products.

Author contributions

Fariba Malekpour Galogahi: conceptualization, experiment, validation, and writing – original draft. Melody Christie: experiment. Ajeet Singh Yadav: experiment. Hongjie An: writing – review & editing and supervision. Helen Stratton: methodology and writing – review & editing. Nam-Trung Nguyen: conceptualization, writing – review & editing, and supervision.

Conflicts of interest

There are no conflicts to declare.

Acknowledgements

This research was funded by an Australian Research Council (ARC) Discovery Project (Grant No. DP220100261). This work was partly performed at the Queensland node-Griffith of the Australian National Fabrication Facility, a company established under the National Collaborative Research Infrastructure Strategy to provide nano- and micro-fabrication facilities for Australian researchers.

References

1 S. Mieszkin, J. F. Yala, R. Joubrel and M. Gourmelon, *J. Appl. Microbiol.*, 2010, **108**, 974–984.
2 L. Paruch, A. M. Paruch, A.-G. Buseth Blankenberg, M. Bechmann and T. Mæhlum, *Acta Agric. Scand., Sect. B*, 2015, **65**, 164–172.
3 X. Bian, F. Jing, G. Li, X. Fan, C. Jia, H. Zhou, Q. Jin and J. Zhao, *Biosens. Bioelectron.*, 2015, **74**, 770–777.
4 K. Ravaliya, J. Gentry-Shields, S. Garcia, N. Heredia, A. Fabiszewski de Aceituno, F. E. Bartz, J. S. Leon and L. A. Jaykus, *Appl. Environ. Microbiol.*, 2014, **80**, 612–617.
5 A. Layton, L. McKay, D. Williams, V. Garrett, R. Gentry and G. Sayler, *Appl. Environ. Microbiol.*, 2006, **72**, 4214–4224.
6 T. K. Yung, K. C. Chan, T. S. Mok, J. Tong, K. F. To and Y. M. Lo, *Clin. Cancer Res.*, 2009, **15**, 2076–2084.
7 S. Lei, S. Chen and Q. Zhong, *Int. J. Biol. Macromol.*, 2021, **184**, 750–759.
8 H. C. Fan, Y. J. Blumenfeld, Y. Y. El-Sayed, J. Chueh and S. R. Quake, *Am. J. Obstet. Gynecol.*, 2009, **200**, 543.
9 T. Hoshino and F. Inagaki, *Syst. Appl. Microbiol.*, 2012, **35**, 390–395.
10 Y. Pan, T. Ma, Q. Meng, Y. Mao, K. Chu, Y. Men, T. Pan, B. Li and J. Chu, *Talanta*, 2020, **211**, 120680.
11 C. Wei, C. Yu, S. Li, J. Meng, T. Li, J. Cheng, F. Pan and J. Li, *Anal. Chem.*, 2022, **94**, 3939–3947.
12 Y. Ren, J. Ji, H. Zhang, L. Cao, J. Hu, F. Xu and Z. Li, *Lab Chip*, 2023, **23**, 2521–2530.
13 D. Xu, W. Zhang, H. Li, N. Li and J.-M. Lin, *Lab Chip*, 2023, **23**, 1258–1278.
14 C. H. Roberts, A. Last, S. Molina-Gonzalez, E. Cassama, R. Butcher, M. Nabicassa, E. McCarthy, S. E. Burr, D. C. Mabey, R. L. Bailey and M. J. Holland, *J. Clin. Microbiol.*, 2013, **51**, 2195–2203.
15 J. Camunas-Soler, H. Lee, L. Hudgins, S. R. Hintz, Y. J. Blumenfeld, Y. Y. El-Sayed and S. R. Quake, *Clin. Chem.*, 2018, **64**, 336–345.
16 I. Abellan-Schneyder, A. J. Schusser and K. Neuhaus, *BMC Microbiol.*, 2021, **21**, 1–14.
17 D. Morisset, D. Stebih, M. Milavec, K. Gruden and J. Zel, *PLoS One*, 2013, **8**, e62583.
18 L. Malic, J. Daoud, M. Geissler, A. Boutin, L. Lukic, M. Janta, A. Elmanzalawy and T. Veres, *Analyst*, 2019, **144**, 6541–6553.
19 S. Zhao, Z. Zhang, F. Hu, J. Wu and N. Peng, *Analyst*, 2021, **146**, 1559–1568.
20 R. Liao, P. Yang, W. Wu, D. Luo and D. Yang, *Environ. Sci. Technol.*, 2018, **52**, 1695–1703.
21 R. Liao, F. Zhao, S. Hamada, P. Yang, H. Xu, D. Luo and D. Yang, *Nano Today*, 2020, **35**, 100958.
22 M. Zhao and N. S. Zacharia, *J. Chem. Phys.*, 2018, **149**, 163326.
23 D. Paunescu, C. A. Mora, L. Querci, R. Heckel, M. Puddu, B. Hattendorf, D. Gunther and R. N. Grass, *ACS Nano*, 2015, **9**, 9564–9572.
24 T. F. Linsenmayer, K. E. Beazley, C. X. Cai, J. P. Canner, J. M. Fitch, J. K. Kubilus, J. M. Millholland, M. Nurminskaya, C. Talbot and N. B. Zak, in *Studies on the Cornea and Lens*, Springer, 2015, ch. 3, pp. 39–66, DOI: 10.1007/978-1-4939-1935-2_3.
25 A. N. Zelikin, A. L. Becker, A. P. Johnston, K. L. Wark, F. Turatti and F. Caruso, *ACS Nano*, 2007, **1**, 63–69.
26 C. A. Juan, J. M. Pérez de la Lastra, F. J. Plou and E. Pérez-Lebeña, *Int. J. Mol. Sci.*, 2021, **22**, 4642.
27 D. Paunescu, M. Puddu, J. O. Soellner, P. R. Stoessel and R. N. Grass, *Nat. Protoc.*, 2013, **8**, 2440–2448.
28 F. Alimirzaei, E. Vasheghani-Farahani, A. Ghiaseddin and M. Soleimani, *J. Tissue Sci. Eng.*, 2017, **8**, 1–10.
29 R. Liao, J. Zhang, T. Li, D. Luo and D. Yang, *Chem. Eng. J.*, 2020, **401**, 126035.
30 L. Pang, G. Abeysekera, K. Hanning, A. Premaratne, B. Robson, P. Abraham, R. Sutton, C. Hanson, J. Hadfield and L. Heiligenthal, *Water Res.*, 2020, **184**, 116192.
31 M. S. Bloch, D. Paunescu, P. R. Stoessel, C. A. Mora, W. J. Stark and R. N. Grass, *J. Agric. Food Chem.*, 2014, **62**, 10615–10620.
32 D. J. Quick and K. S. Anseth, *J. Controlled Release*, 2004, **96**, 341–351.
33 M. Fujiwara, K. Shiokawa, K. Hayashi, K. Morigaki and Y. Nakahara, *J. Biomed. Mater. Res., Part A*, 2007, **81**, 103–112.
34 Y. J. Eun, A. S. Utada, M. F. Copeland, S. Takeuchi and D. B. Weibel, *ACS Chem. Biol.*, 2011, **6**, 260–266.

35 F. M. Galogahi, Y. Zhu, H. An and N.-T. Nguyen, *J. Sci.: Adv. Mater. Devices*, 2020, **5**, 417–435.
36 E. Vazquez, D. M. Dewitt, P. T. Hammond and D. M. Lynn, *J. Am. Chem. Soc.*, 2002, **124**, 13992–13993.
37 N. Jessel, M. Oulad-Abdelghani, F. Meyer, P. Lavalle, Y. Haikel, P. Schaaf and J. C. Voegel, *Proc. Natl. Acad. Sci. U. S. A.*, 2006, **103**, 8618–8621.
38 Y. Temiz, R. D. Lovchik, G. V. Kaigala and E. Delamarche, *Microelectron. Eng.*, 2015, **132**, 156–175.
39 F. M. Galogahi, Y. Zhu, H. An and N.-T. Nguyen, *Microfluid. Nanofluid.*, 2021, **25**, 1–11.
40 S. Hiranphinyophat, A. Otaka, Y. Asaumi, S. Fujii and Y. Iwasaki, *Colloids Surf., B*, 2021, **197**, 111423.
41 S. C. Yang, H. X. Ge, Y. Hu, X. Q. Jiang and C. Z. Yang, *J. Appl. Polym. Sci.*, 2000, **78**, 517–526.
42 M. N. Hatori, S. C. Kim and A. R. Abate, *Anal. Chem.*, 2018, **90**, 9813–9820.
43 H. Becker, *Lab Chip*, 2009, **9**, 2119–2122.
44 H. Y. Tan, W. K. Loke and N.-T. Nguyen, *Sens. Actuators, B*, 2010, **151**, 133–139.
45 J. Sivasamy, T.-N. Wong, N.-T. Nguyen and L. T.-H. Kao, *Microfluid. Nanofluid.*, 2011, **11**, 1–10.
46 F. M. Galogahi, A. Ansari, A. J. Teo, H. Cha, H. An and N.-T. Nguyen, *Biomed. Microdevices*, 2022, **24**, 40.
47 A. S. Yadav, F. M. Galogahi, A. Vashi, C. H. Ooi, S. K. Rajan and N.-T. Nguyen, *Lab Chip*, 2023, DOI: **10.1039/D3LC00337J**.
48 N. Rahman, M. A. Khan, R. A. Khan and T. A. Chowdhury, *Polym.-Plast. Technol. Eng.*, 2011, **50**, 404–411.
49 S. Ghasaban, M. Atai, M. Imani, M. Zandi and M. A. Shokrgozar, *J. Biomed. Mater. Res., Part A*, 2011, **99**, 240–248.
50 A. Petropoulou, M. Dimitriadi, S. Zinelis, A. Sarafianou and G. Eliades, *Materials*, 2020, **13**, 2540.
51 T. Y. Lee, T. M. Choi, T. S. Shim, R. A. Frijns and S. H. Kim, *Lab Chip*, 2016, **16**, 3415–3440.
52 C. Zhou, P. Zhu, X. Han, R. Shi, Y. Tian and L. Wang, *Lab Chip*, 2021, **21**, 2684–2690.
53 X. Han, T. Kong, P. Zhu and L. Wang, *Langmuir*, 2020, **36**, 8165–8173.
54 H. Kalman, *Rev. Chem. Eng.*, 2022, **38**, 149–165.